UDK 621.3:(53+54+621+66), ISSN0352-9045 Informacije MIDEM 23(1993)4, Ljubljana

CROSS-SECTIONAL SCANNING TUNNELING MICROSCOPY ON HETEROSTRUCTURES: ATOMIC RESOLUTION, COMPOSITION FLUCTUATIONS AND DOPING

M.B. Johnson and H.W.M. Salemink
IBM Research Division, Zurich Research Laboratory, Ruschlikon, Switzerland

INVITED PAPER
21st International Conference on Microelectronics, MIEL'93
29th Symposium on Devices and Materials, SD'93
September 29 - October 1, 1993, Bled, SLOVENIA

Key words: semiconductors, STM scanning tunneling microscopy, analysis, structural properties, chemical properties, electronic properties, spatial dimensions, atomic scale, nanometer scale, Al-Ga-As-Ga-As heterostructure, measurements, dopants, UHV ultrahigh vacuum, experimental results

Abstract: Cross-sectional scanning tunneling microscopy on semiconductor structures is evolving into a technique to analyze structural, chemical, and electronic properties on the atomic and nanometer scale in all spatial dimensions, in particular in the lateral and in-depth spatial dimensions of the structure. This technique has been used on the ultrahigh vacuum cleaved (110) plane of (001)-grown AlGaAs/GaAs heterostructures. We report on measurements of i) interface roughness, as well as alloy fluctuations and ordering; ii) the variation of electronic properties over an interface as well as fluctuations within the alloy; and iii) the distribution of individual dopant sites.

Rasterska tunelska mikroskopija presekov heteroslojnih polprevodnikov: atomska ločljivost, sestava, fluktacije in dopiranje

Ključne besede: polprevodniki, STM mikroskopija skanirna tunelna, analiza, lastnosti strukturne, lastnosti kemične, lastnosti elektronske, dimenzije prostorske, skala atomska, skala nanometerska, Al-Ga-As-Ga-As heterostrukture, meritve, dopanti, UHV vakum ultravisoki, rezultati eksperimentalni

Povzetek: Rasterska tunelska mikroskopija presekov polprevodniških struktur se razvija v tehniko, ki bo sposobna analizirati strukturne, kemične in elektronske lastnosti na atomski in nanometrski skali v vseh prostorskih dimenzijah, še posebej v lateralni in vertikalni prostorski dimenziji raziskovane strukture. Omenjeno tehniko smo uporabili na vzorcih AlGaAs/GaAs z orientacijo (001) na površini razcepljeni v smeri (110) in pripravljeni v ultravisokem vakuumu. V delu prikazujemo meritve i) hrapavosti površine kakor tudi fluktuacijo urejenosti in sestave legure, ii) spremembe elektronskih lastnosti po površini kakor tudi znotraj legure in iii) porazdelitev posameznih atomov dopantov

1. Introduction:

As semiconductor devices become smaller, knowledge of the electronic properties on the nanometer scale and of the crystallographic and chemical structure on the atomic scale will be of paramount importance in all dimensions. However, conventional analytical tools do not readily afford this knowledge on such a scale. For example in molecular beam epitaxial (MBE) growth, electron diffraction is usually used during epitaxy to monitor the layer-by-layer growth,[1] whereas high-resolution transmission electron microscopy (TEM)[2] and X-ray diffraction[3] are used to determine the structure after growth. These techniques, however, produce crystallographic information averaged over many lattice unit cells. The electronic parameters of such structures are often derived from photoluminescence[4] and photoemission[5] which measure semiconductor properties related to the band structure (eg. valence-band offset and band gap), including their variation across interfaces, but again averaged over many lattice unit cells in volume or a large surface area. Analysis of electronic properties of device structures by capacitance-voltage (C-V) or current-voltage (I-V) probes and spreading resistance profiling (SRP) require modeling and are difficult to extend to the lateral dimensions.[6] Similarly, analysis of electronic properties of devices by means of the device performance itself requires sophisticated modeling, and the determination of the physical characteristics is difficult. Finally, chemical profiling techniques such as secondary ion mass spectroscopy (SIMS) and Auger electron spectroscopy (AES) are limited to a depth resolution in the range of 5 nm and are difficult to extend to lateral dimensions.[6] On the other hand scanning tunneling microscopy (STM)[7-9] is an extremely surface- sensitive tool with atomic lateral res-

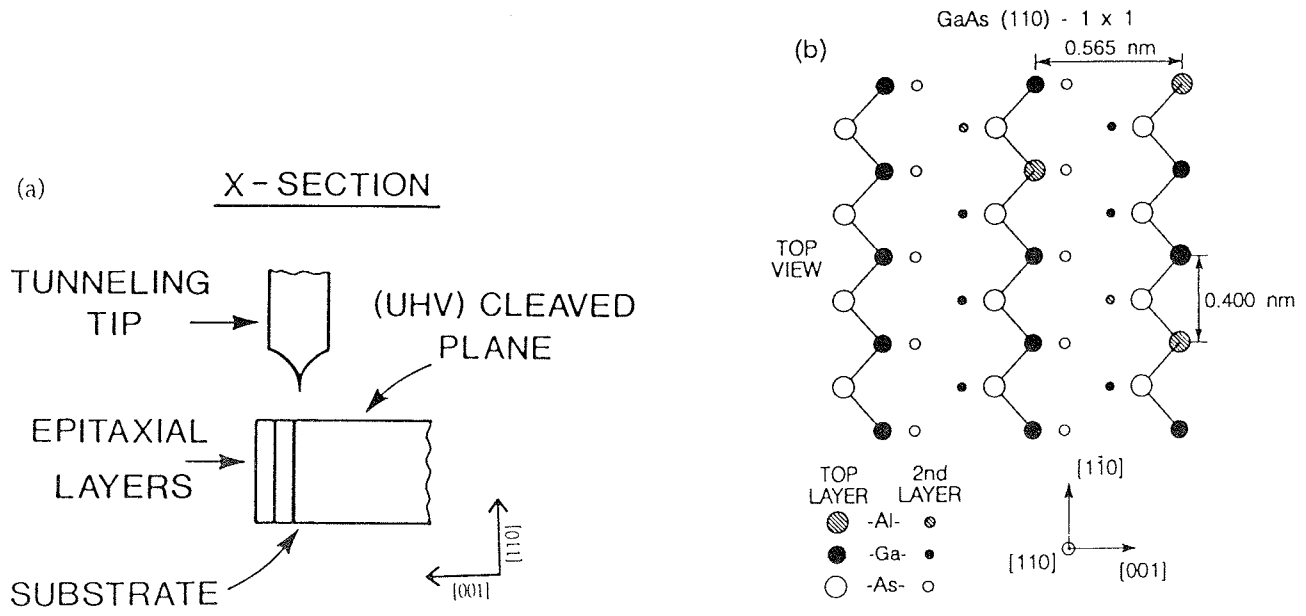

Fig. 1: (a) Sketch of cross-sectional STM on heterostructures. /© 1991 Elsevier Science Publishers B.V./ (b) Top view of atomic arrangements of the group-III Ga and Al and group-V As sites on the (110) face. Tunneling can be out of the group-V valence As states or into the group-III conduction states by negative and positive sample voltage. The [001] and [110] directions and dimensions are shown. The distance to the next monolayer in the (110) plane is 0.2 nm. /© 1990 John Wiley & Sons, Inc./

olution and sensitivity to crystallographic, chemical and electronic information. Thus when used on a suitable cross-sectional surface, STM can yield structural, chemical, and electronic information in the depth and lateral dimensions with unprecedented resolution. Hence there is growing interest in the analysis of epitaxially grown multilayers by cross-sectional STM (XSTM).[10-18] Figure 1(a) shows the XSTM configuration. The preparation of this cross-sectional surface is a crucial requirement for successful application of XSTM. The best results require an atomically flat, uncontaminated surface. This is readily achieved in the III-V materials system with a (110) facet cleaved in ultrahigh vacuum (UHV). The work of this paper concerns AlGaAs/GaAs heterostructures (see Fig. 1(b)) where we demonstrate: i) spatial resolution and chemical sensitivity on an atomic scale, which allows the measurement of interface roughness, as well as alloy fluctuations and ordering; ii) electronic sensitivity on a near-atomic scale, which allows the measurement of the variation of band structure within alloys and across interfaces; and iii) the direct sensitivity to dopants, which allows the determination of dopant density. The extension of this work to other heterostructure systems, such as Si and SiGe, depends principally on the generation of a cross-sectional surface that is atomically flat and uncontaminated.

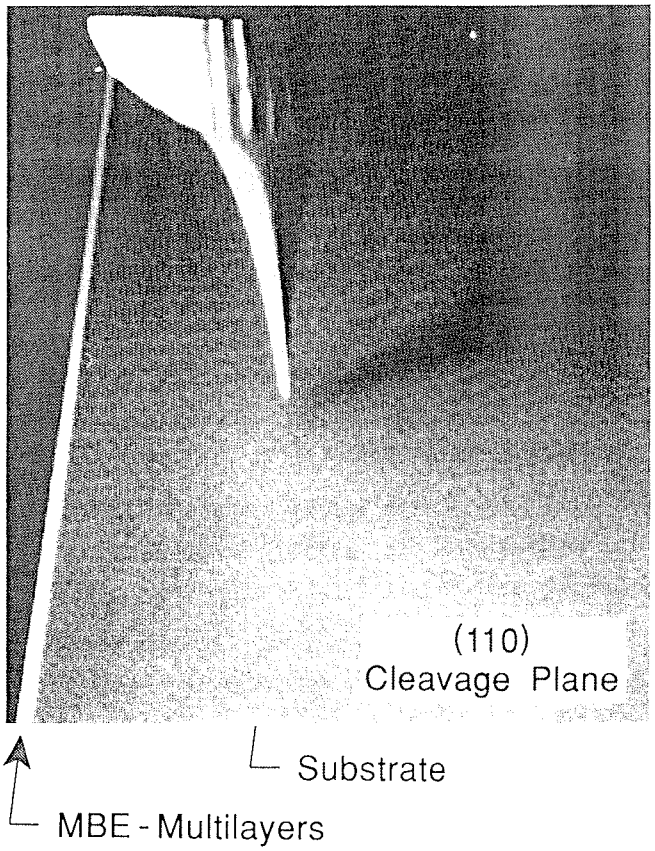

Fig 2: Secondary electron SEM image of tunneling tip in approach to cleaved multilayer stack. In the (110) cleaved cross section, the multilayer stack is seen as a white stripe to the left of the (gray) substrate (see also Fig. 1a). Note the tip shadow on the substrate due to blocking of the electron beam. This effect at close proximity ($\cong 1.0\ \mu m$) is used to guide the tip towards the multilayer stack (SEM magnification factor is 10 K).

2. Experimental

The results described in this paper are obtained with two UHV-STM's: one early system built into a UHV-compatible SEM (scanning electron microscope),[19] and a second version with optical access instead of the SEM. Both STM's have been successfully used to study cross

sections of nanometer-size, MBE-grown multilayer structures. The SEM is used for three purposes: i) to evaluate the apex shape of the tunneling tip, ii) to analyze the suitability of the particular cleavage plane under study and iii) to guide the STM tip into the area of interest within the heterostructure stack, typically with a positional accuracy of 25 nm. Figure 2 shows an SEM image of the tunneling tip in approach to the cleaved sample. An iterative method for guiding the tip to the edge[18] using reliable positioning piezo-sliders as well as more reliable tip preparation and sample cleaving methods have largely replaced the use of SEM in recent work. Pressure in the STM environments is $<4 \times 10^{-11}$ mbar. The GaAs/AlGaAs multilayer samples were grown by MBE on (001) GaAs substrates. The results described here are for highly-doped p-type (Be) samples with dopant concentration ranging from 1 to -10 x 10^{18} cm^{-3} and Al concentration in the alloy typically $Al_xGa_{1-x}As$ with x=0.30 to 0.35. Various different structures are used in the stack, and several repetitions of the stack are grown to facilitate the location of the structure of interest. Atomic resolution on III-V heterojunctions became routine after several improvements were made, notably i) thinning back the substrate to 150 μm by mechanical polishing (to facilitate the (110) cleaving across the stack), ii) use of lower tunneling current (0.1 nA or lower) and more highly doped samples and iii) optimization of the tip preparation procedure.[20]

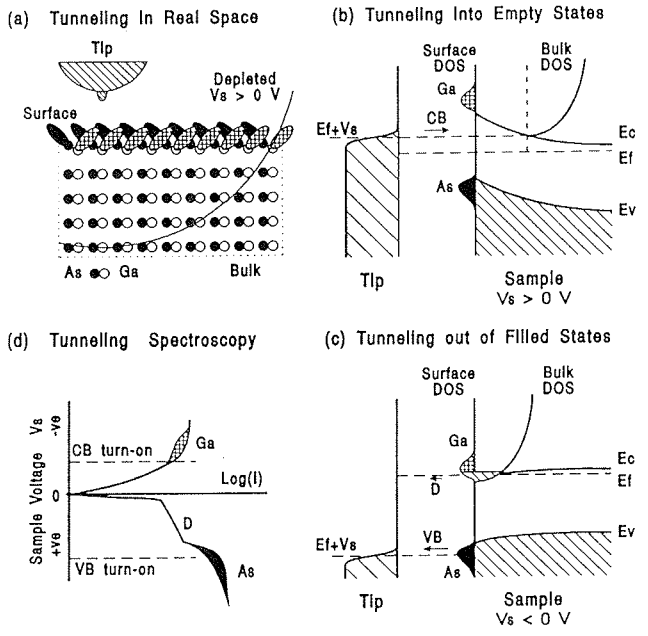

Fig 3: Schematic views of STM tunneling on n-type GaAs (clockwise). (a) Tunneling between tip and sample in real space. (b) Tunneling energy diagram for sample voltage > 0 sensitive to empty Ga and Al states; also sketched is the tip-induced band-bending with the semiconductor in depletion. (c) Tunneling energy diagram for sample voltage < 0 sensitive to filled As states; also sketched is the tip-induced band-bending with the semiconductor in accumulation. (d) Schematic current-voltage characteristic with contributions from VB and CB; D shows tunneling via dopant levels. From /26/.

The atomic arrangement on the (110) cleavage plane (top view) is drawn in Fig. 1(b). Note that for AlGaAs material a fraction of the group-III sites is replaced. On the charge-neutral (110) plane the group-III and V atoms maintain their valence character. As a result the filled (group V) and empty (group III) states can be sensed by tunneling out of or into the sample[8] as shown in Fig. 3. In addition the valence and conduction band (VB and CB) turn-ons can be determined with respect to E_F via simultaneous current voltage spectroscopy.[21, 22] Spectroscopy on the clean UHV cleaved III-V (110) surface displays both VB and CB band onsets and a gap region of approximately 1.45 eV, free of surface states, as reported previously.[21]

3. Results and Discussion

In this work we describe four different sets of STM measurements, each associated with various aspects of GaAs/AlGaAs heterostructures. They are: i) filled-state images that show Al sensitivity and hence interface roughness as well as alloy fluctuations and ordering. Furthermore these images allow the determination of the layer metrology by STM and this is compared to that obtained with HRTEM; ii) filled-state images in combination with I-V spectroscopy that are sensitive to the variation of the band structure across a AlGaAs/GaAs interface and within the AlGaAs layer; and iii) filled-state images of a Be-doped GaAs buffer layer, of a Zn-doped GaAs substrate, and of a Be-doped sample with variable doping concentrations that are directly sensitive to the electronically active dopant atoms and allow the direct measurement of dopant density.

An STM image of a heterostructure stack consisting of a series of adjacent, equally thick pairs of $Al_{0.3}Ga_{0.7}As$/GaAs layers of 10, 5, 2, and 1 nm thickness is shown in Fig. 4./see Ref. 23/ Figure 4(a) shows the bulk-band diagram for the stack. Figure 4(b) shows an area of nearly 30 x 50 nm with all layers in one period of the stack clearly displayed. The image was taken with a sample voltage of -2.1 V and a demand current of 0.1 nA, thus probing the As-related filled states.[8] Note that atomic corrugation is apparent in both the [001] and [110] directions. In the image in Fig. 4(b) the GaAs regions are uniform, while the AlGaAs ternary regions have a mottled texture.[24] Several types of localized features are present in the layers, but the discussion here concerns the clean regions. Figure 4(c) shows that the topographic corrugation on line C-C' of Fig. 4(b) extends through one period of the stack along the [001] direction away from localized contamination features. In the GaAs regions the corrugation is regular with an amplitude of 0.03 nm, while in the 10 and 5 nm thick AlGaAs layers the corrugation is irregular and the layers appear nearly 0.1 nm lower than the surrounding GaAs. The smaller 2 and 1 nm thick AlGaAs layers are observ-

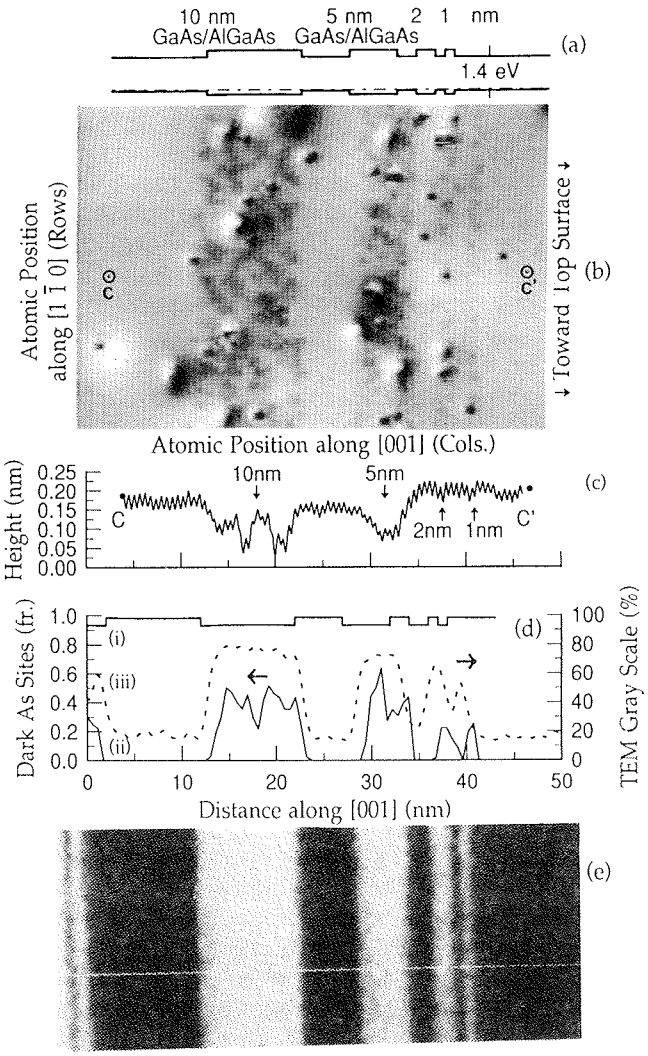

Fig. 4: Large-scale STM image of a (110)-cleaved GaAs/AlGaAs heterostructure stack. (a) Calculated bulk-band structure for the as-grown heterostructure. (b) Topographic image of the stack taken with a sample voltage of -2.1 V and a demand current of 0.1 nA. The image is nearly 50 x 50 nm and the As sublattice is indexed along the [110] and [001] directions. The relative tip height is represented by a gray scale, from 0 (black) to 0.43 nm (white). (c) Topographic corrugation along line C-C' in registry with that displayed in (b). (d) Comparison of STM with dark-field TEM. (i) Intended growth plan. (ii) TEM gray scale across layers from dark- field image (e) (iii) Fraction of dark As sites along a [110] corrugation line in the neighborhood of C-C' versus position along the [001] direction. (e) TEM dark-field image of the stack in registry with (d). From /23/.

able, but their contrast is much less than that of the two thicker layers. Note that this height variation is not real topography because there are no atomic steps on the surface; instead, it is electronic in nature. The regular corrugation in the GaAs is the result of the homogeneous As surface site bonding configuration there. In contrast, the bonding configuration of As surface sites in the ternary AlGaAs is variable depending on the number of Al nearest-neighbor sites. Because the Al-As bond is more ionic than the Ga-As bond, Al nearest-neighbors result in more charge being transferred to the nearest As sites, thereby lowering the energy and changing the spatial extent of the As-related surface state. Thus the As corrugation fluctuates depending on the number of Al atoms bonded to the surface As. Conversely the fluctuation of the As corrugation indicates a variation of the number of Al atoms bonded to the surface As. The apparent topographic lowering in the thicker AlGaAs layers is the result of the different electronic properties of the barrier region; it most probably occurs because the barriers are completely depleted, which requires the tip to approach the surface. The distance over which this apparent height varies from GaAs to the AlGaAs - about 3-4 [001] corrugations - and the lack of contrast in the 1 and 2 nm barrier is consistent with the expected wave function penetration of the holes from the quantum wells into the barriers that result from the near-atomic scale variation of band offsets.

Figure 5 shows an expanded image of the 10 nm thick AlGaAs layer. The occurrence of dark or light bands 3-4 lattice spacings in width (about 2 nm) extending in the [112] and [1̄12] directions is clearly visible (it is also displayed in parts of the 5 nm layer). This suggests that

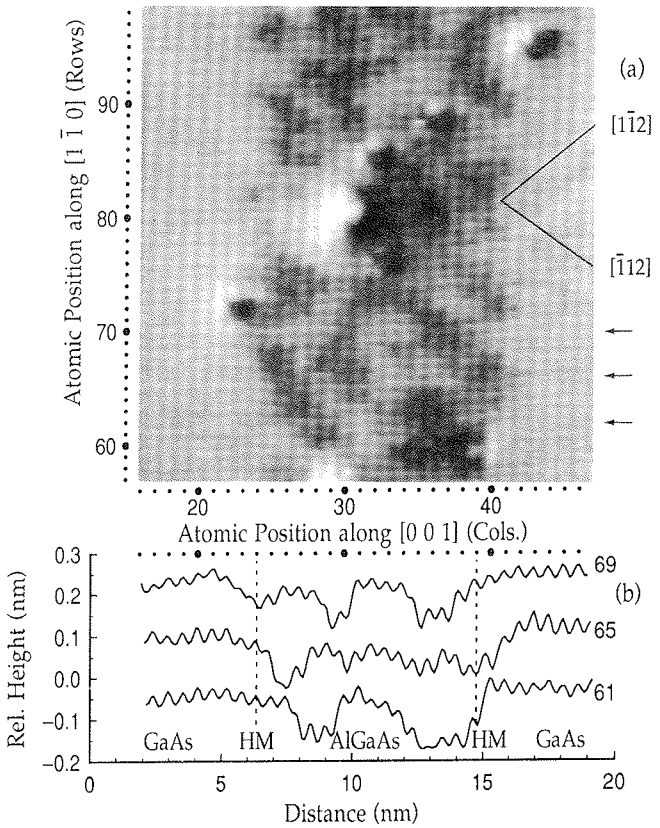

Fig. 5: Expanded STM image of 10 nm AlGaAs layer in Fig. 4 (a) Topographic image of an area of about 20 x 20 nm; relative tip height represented by a gray scale from 0 (black) to 0.38 nm (white). The [112] and [1̄12] directions are indicated. (b) Topographic line scans along rows 61, 65, and 69 as indicated. The positions of the half- maximum of the AlGaAs layer are indicated by HM. From /23/

Al-rich regions nucleate at the GaAs/AlGaAs interface in isolated positions and grow preferentially. The interfaces shown in Fig. 5 also have roughness on this 2 nm length scale. This is in agreement with measurements made by other techniques.[2]

Finally, we consider quantitative metrology of these layers on the (sub-)nanometer scale. Let us consider selected contamination-free regions in the image in Fig.4(b) that span the entire superlattice period in a piecewise manner near line C-C'. From these regions we can determine the fraction of dark As sites along the [110] row in this area. In Fig. 4(d) curve (iii) shows this fraction of dark As positions plotted versus its position along the [001] direction - typically more than 30 sites per vertical line are counted. This fraction of dark As positions is indicative of the Al fraction, and is sufficient for estimating the actual thickness of the layers grown, as shown. Curve (ii) is the percentage gray scale from the TEM dark field image shown in Fig. 4(e) which is also indicative of Al content. And finally, curve (i) indicates the intended growth plan for the stack. Comparing curves (ii) and (iii) (STM and TEM) shows 4% agreement in the layer thickness's which is reasonable, considering that different parts of the wafer were measured. Note the TEM and STM-measured GaAs layers are systematically longer than the matching AlGaAs layer.

Local I-V curves can be acquired simultaneously with the topography to assess the transition in the electronic band structure across the GaAs- AlGaAs interface. /see Ref. 22/ In Fig. 5(a) the filled-state image of an interface is shown together with the sampling points for the I-V curves at a 1.5 nm grid. In the interest of high stability in spectroscopy, topographic resolution is traded off slightly. A set of I-V curves from a line across the interface is shown in Fig. 5(b) and the transition region is noted by the drop in the VB turn-on voltage. The observed VB turn-on energy is plotted as a function of distance to the interface in Fig. 5(c) together with the calculated positions for the bulk (C) and surface (S) VB edge energy. The tip-induced electrostatic depletion of the semiconductor is explicitly taken into account in curve (S).[22] The lack of change at the CB onset is somewhat surprising and possibly due to interference with surface states. Note the fluctuations in the VB edge in the AlGaAs from the experimental data: this might reflect the local variation of the VB edge energy due to the Al fluctuations (Fig. 4) and the effect of the lateral extent of the depletion region present during spectroscopy measurements /.Fig. 1(a)/. The data in Fig. 5 demonstrate the measurement of electronic band parameters on a near-atomic scale in semiconductor structures.

Figure 7 shows a filled-state image of a Be doped p-type GaAs MBE-grown buffer layer with p =1 x 10^{19} cm^{-3}. /see Ref. 25/ Nine hillock features are observed scattered throughout the 31 x 29 nm scan and labeled on the perimeter of the image. Figure 7(b) shows corrugation traces across several of these hillock features in [001] and [110] directions. In Fig. 7(b) the hillocks have a height of up to 0.02 nm and a diameter of about 2

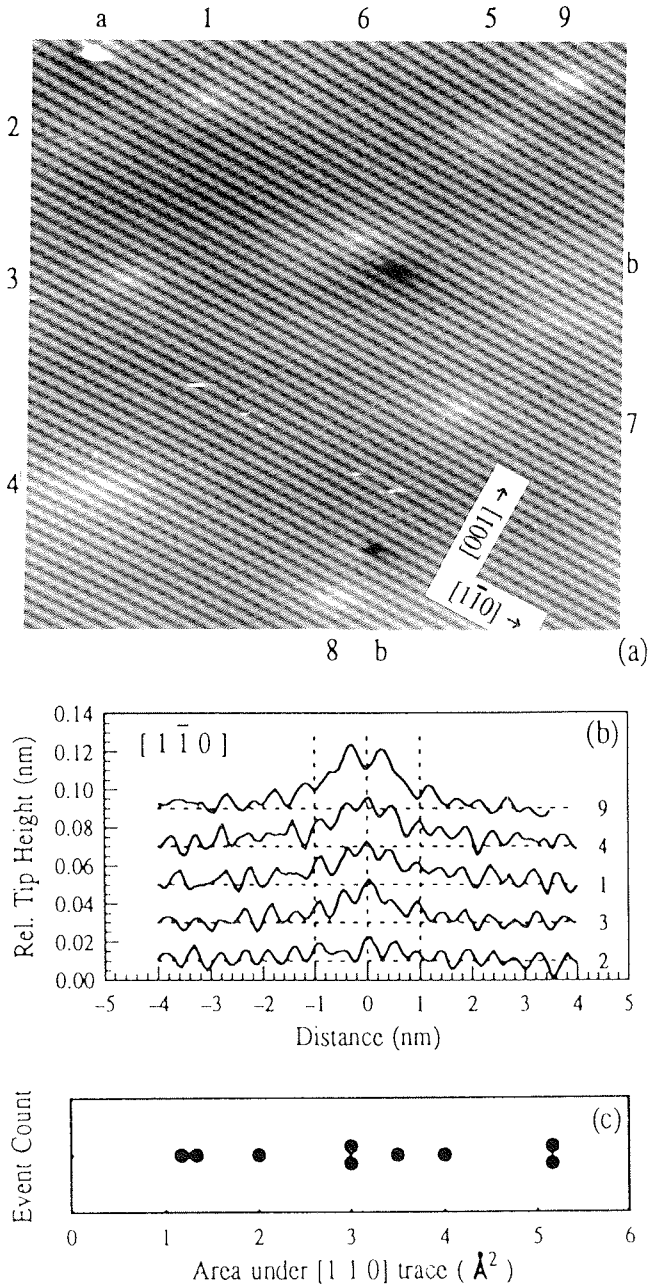

Fig. 7: (a) STM image of a (110)-cleaved, 1 x 1^{19} cm^{-3}, Be-doped GaAs surface. Image displays 31 x 29 nm of the As sublattice taken with sample voltage -2.1 V and demand current 0.1 nA. The relative tip height is represented by a gray scale from 0 (black) to 0.2 nm (white). Nine hillocks (dopants) are identified using numbers at the closest point on the perimeter. (b) Tip height traces along the [110] direction of a selection of the hillocks identified in (a). (c) Scatter plot of area under the [110] tip height traces (integrated intensity) of all nine hillocks - note the uniform distribution. From /25/

nm.[25,26] These hillocks correspond to the enhancement of the surface density of states expected in the neighborhood of Be acceptor sites which gives rise to a slight increase of the tip-surface distance as observed. The observed diameter - roughly the size of the acceptor

Bohr radius (2.5 nm) - and height of these hillocks are in agreement with calculations of the change in the surface density of states due to a nearby dopant and its effect on tunneling process. At a doping density of 1 x 10^{19} cm^{-3} in the area shown in Fig. 7(a) one expects two dopant atoms per monolayer. Thus the observation of nine hillocks indicates a sensitivity to dopant atoms in the top five monolayers corresponding to about 1 nm (the distance between monolayers is 0.2 nm in the [110] direction). This is in agreement with the acceptor Bohr radius and the calculations described above.[27]

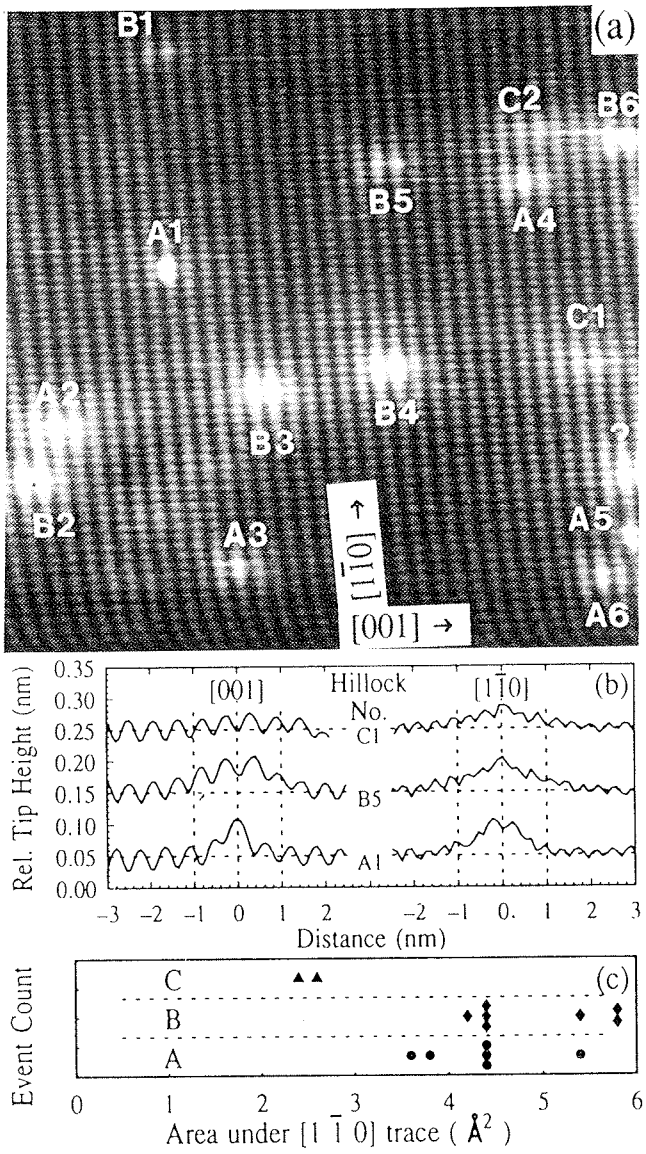

Fig. 8: (a) STM image of a (110)-cleaved, 5 x 10^{19} cm^{-3}, Zn-doped GaAs surface. Image displays 20 x 28 nm of the As sublattice taken with sample voltage -2.1 V and demand current 0.1 nA. The relative tip height is represented by a gray scale from 0 (black) to 0.2 nm (white). Six type A hillocks, six type B hillocks, and one type C hillock are identified with numbers. (b) Tip height traces along the [110] and [001] directions of a selection of the hillocks of type A, B, and C identified in (a). (c) Scatter plot of area under the [110] tip height traces (integrated intensity) or all hillocks labeled. From /25/

Figure 8 shows a filled-state image of a very highly-Zn doped p-type GaAs substrate buffer layer with p =5 x 10^{19} cm^{-3}. /see Ref. 25/ Many hillock features are scattered throughout the 20 x 28 nm scan. The prominent hillock features are labeled A, B and C according to their symmetry. Corrugation traces of examples of each of these types of hillock in [001] and [110] directions are shown in Fig. 8(b). The diameter and height of these hillocks are similar to those observed above for the Be-doped buffer layer. Moreover in this case, the number and symmetry of the features indicate that hillock feature A corresponds to a dopant in the top layer, feature B to a dopant in the second layer and C to a dopant in a still deeper layer. Thus the dopant can be localized in all three dimensions with atomic precision.

An STM image of a heterostructure modulation-doped stack consisting of 100 nm thick layers of Be-doped GaAs between 2.5 nm thick AlGaAs marker layers is shown in Fig. 9. /see Ref. 28/ Figure 9(b) is a large-scale STM image and (c)-(f) present a series of depth profiles (along the growth direction) over a single set of the modulation-doped layers. Figure 9(b) shows the 100 x 50 nm STM topographic image of a set of GaAs layers including the AlGaAs marker layers (spotted dark vertical lines) imaging the filled As states. Above and in registry with Fig. 9(b), Fig. 9(a) shows the intended growth plan including Be concentration, growth interruptions (marked GI), and the delta-doped layer (marked δ). Figure 9(c) shows several horizontal line scans taken across Fig. 9(b) at the positions indicated. Note that atomic corrugation is observed throughout the STM image as indicated in the inset (enlarged 5x). In the STM image /Fig. 9(b)/ the dark spots are cleave-induced As vacancies[5] and are not of interest here. The white spots indicate individual ionized dopants in the top several atomic layers. They are typically 2 nm in diameter and about 0.05 nm in height as shown above. The overall contrast - dark in the middle and bright on the sides - is due to the tip approaching the sample by about 0.1 nm in the low doped region in the middle of the image as indicated by the line scans in Fig. 9(c). Figure 9(f) shows SIMS and C-V profiles of a typical set of the GaAs layers between the AlGaAs markers. Figure 9(d) plots a line scan corresponding to the average of all the line scans making up the top half of the image in Fig. 9(b). Figure 9(e) is a histogram plot of the white spots (ionized dopant sites) counted in 10-nm- wide vertical stripes between the marker layers versus horizontal position along with the SIMS data (dotted) for comparison. The disagreement between the intended doping and the SIMS data is due to the segregation to the surface, and to bulk diffusion of the Be during growth. The SIMS plot is thought to reflect the actual Be concentration. Figure 9(d) shows qualitative agreement between the linear plot of the average tip height and the logarithmic plot of the Be concentration. The average tip height is sensitive to the dopant concentration because the surface band bending under the tunneling tip that affects the tip height is governed by the dopant concentration. The histogram of the Be dopant sites in Fig. 9(e) shows quantitative agreement with the SIMS Be concentration. This agree-

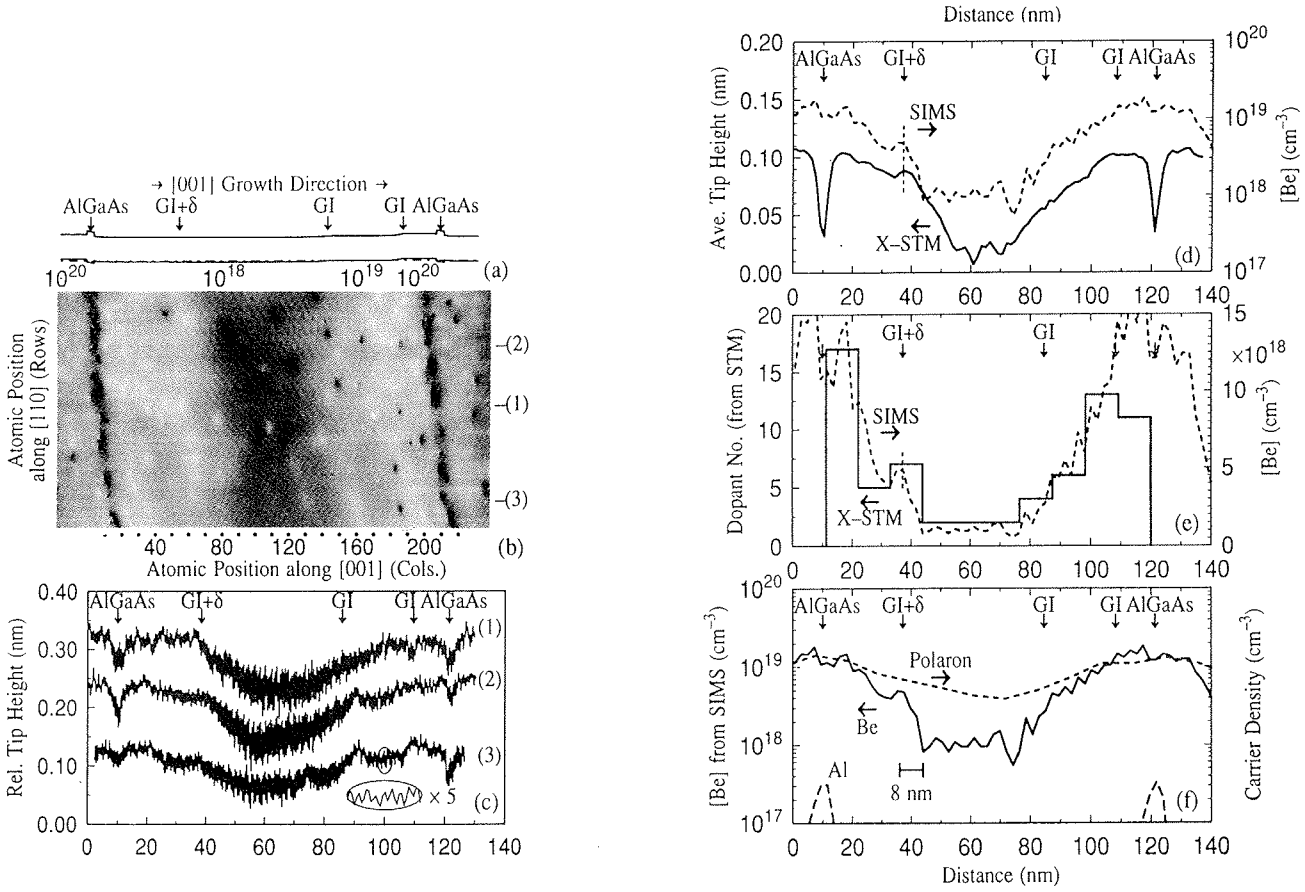

Fig. 9: Large-scale STM image of GaAs layers with variable dopant concentration and various depth profiles. (a) Calculated bulk-band structure for the intended heterostructure. In registry below, (b) shows the topographic image, 100 x 50 nm in size, of the layers taken with sample voltage -2.1 V and demand current 0.1 nA. The relative tip height is represented by a gray scale from 0 (black) to 0.2 nm (white). (c) Several topographic line scans across the image (b) along the [100] direction with the AlGaAs layers vertically aligned.Note the atomic corrugation shown in inset. (d) Line scan (solid) corresponding to the averaged line scan over the top half of Fig. 1(b) taking the slight drift into account. The line scan is smoothed slightly to remove atomic corrugation and is compared to the Be concentration measured by SIMS (dotted, right log. axis). (e) Dopant histogram determined by counting the white hillocks (dopants) in a series of rectangles across (b) (solid, left linear axis) and compared to the measured Be concentration measured by SIMS (dotted, right linear axis). (f) Be concentration (solid) and Al counts (dotted) measured by SIMS as well as dopant concentration determined by Polaron C-V analysis (dashed). From /28/

ment is for a sensitivity of the STM to the top 1 nm as was observed above. Thus both the dopant number and the relative tip height can be used to indicate the dopant concentration. The former shows the actual position of the dopant while the latter shows the behavior of the bands at the surface which is sensitive to the carrier concentration. Note the weak signature of the delta-doped layer is observed in the SIMS profile, the average tip height profile in Fig. 9(d), and dopant number histogram in Fig. 9(e). Thus STM appears to be an ideal tool for the study of such delta-doped layers.

4. Summary

Cross-sectional STM on heterostructures is evolving into a technique to analyze structural and electronic properties on the atomic and nanometer scale in all spatial dimensions. Because of the cross-sectional aspect involved, this represents both lateral and in-depth spatial dimensions. Other conventional techniques average one or more dimensions over a given length scale. In this work on the (110) plane of (001)-grown III-V heterostructures this high-resolution capability has been used to measure directly: i) interface roughness as well as alloy fluctuations and ordering; ii) the variation of electronic properties over an interface as well as fluctuations within the alloy; and iii) the distribution of individual dopant sites. In the future, such issues as incorporation of bulk and delta doping as well as their interdiffusion in III-V materials can be investigated. The extension of this technique from III-V materials to other heterostructure systems, such as Si and SiGe structures, is critically dependent on the preparation of a suitable cross-sectional surface.

Acknowledgments

We acknowledge the MBE growth provided by H.P. Meier, expert sample preparation by L. Perriard and H. Richard, technical assistance from U. Maier, STM software provided by B. Michel, transmission electron microscopy provided by R. Broom, and SIMS analysis provided by F. Cardone.

REFERENCES

1. J.M. van Hove, P.I. Cohen, J. Cryst. Growth **81**, 13 (1987).

2. A. Ourmazd, D.W. Taylor, J. Cunningham and C.W. Tu, Phys. Rev. Lett. **62**, 933 (1989).

3. J.M. Vandenberg, R.A. Hamm, M.B. Panish, and H. Temkin, J. Appl. Phys. **62**, 1278 (1987).

4. B.G. Streetman and Y.C. Shih, J. Vac. Sci. Technol. B **10**, 296 (1992).

5. E.T. Yu, D.H. Chow, and T.C. McGill, Phys. Rev. B **38**, 12764 (1988).

6. See Proc. of the First Int'l Workshop on the Measurement and Characterization of Ultra-shallow Doping Profiles in Semiconductors, J. Vac. Sci. Technol. B **10**, (1992). In particular W. Vandervorst and T. Clarysse, J. Vac. Sci. Technol. B **10**, 302 (1992).

7. G. Binnig, Ch. Gerber, H. Rohrer, and E. Weibel, Phys. Rev. Lett. **49**, 57 (1982).

8. R.M. Feenstra, J.A. Stroscio, J. Tersoff, and A.P. Fein, Phys. Rev. Lett. **58**, 1192 (1987).

9. R.J. Hamers, R.M. Tromp, and J.E. Demuth, Phys. Rev. Lett. **56**., 1972 (1986).

10. S. Hosaka, S. Hosoki, K. Takata, K. Horiuchi, and N. Natsuaki, Appl. Phys. Lett. **53**, 487 (1988).

11. S. Kordic, E.J. van Loenen, D. Dijkkamp, A.J. Hoeven, and H.K. Moraal, J. Vac. Sci. Technol. A **8**, 549 (1990).

12. H.W.M. Salemink and O. Albrektsen, J. Vac. Sci. Technol. B **10**, 1799 (1992).

13. P. Muralt, Appl. Phys. Lett. **49**, 1441 (1986).

14. P. Muralt, H. Meier, D.W. Pohl, and H.W.M. Salemink, Appl. Phys. Lett. **50**, 1352 (1987).

15. H.W. Salemink, H.P. Meier, R. Ellialtioglu, J.W. Gerritsen, and P.R. Muralt, Appl. Phys. Lett. **54**, 1112 (1989).

16. R.M. Feenstra, E.T. Yu, J.M. Woodall, P.D. Kirchner, C.L. Lin, and G.D. Pettit, Appl. Phys. Lett. **61**, 795 (1992).

17. M.B. Johnson and J.M. Halbout, J. Vac. Sci. Technol. B **10**, 508 (1992).

18. E.T. Yu, M.B. Johnson, and J.-M. Halbout, Appl. Phys. Lett. **61**, 201 (1992).

19. Ch. Gerber, G. Binnig, H. Fuchs, O. Marti and H. Rohrer, Rev. Sci. Instrum. **57**, 221 (1986); Vacuum Generators VG-HB 100 Multilab UHV-SEM/SAM.

20. O. Albrektsen, K.A. Mörch, A.R. Thölen and H. Salemink, in preparation.

21. R.M. Feenstra and J.A. Stroscio, J. Vac. Sci. Technol. B **5**, 923 (1987).

22. H.W.M. Salemink, O. Albrektsen, and P. Koenraad, Phys. Rev. B **45**, 6946 (1992).

23. M.B. Johnson, U. Maier, H.-P. Meier, and H.W.M. Salemink, Appl. Phys. Lett. **63**, 1273, (1993).

24. O. Albrektsen, D.J. Arent, H.P. Meier, and H.W.M. Salemink, Appl. Phys. Lett. **57**, 31 (1990).

25. M.B. Johnson, O. Albrektsen, R.M. Feenstra, and H.W.M. Salemink, Appl. Phys. Lett. **63**, 2923, (1993).

26. M.B. Johnson, H. Salemink, O. Albrektsen and E.T. Yu, Proc. of 7th Int'l Winter School, Mauterndorf, Austria, February 24-28, 1992, in "Low- Dimensional Electronic Systems," edited by G. Bauer, F. Kuchar and H. Heinrich (Springer-Verlag, Berlin, 1992) pp.108-119.

27. S.M. Sze, Physics of Semiconductor Devices, 2nd Edition, (Wiley, New York, 1981).

28. M.B. Johnson, H.P. Meier, and H.W.M. Salemink, Appl. Phys. Lett. **63**, 3636, (1993).

M.B. Johnson and H.W.M. Salemink
IBM Research Division, Zurich Research Laboratory,
8803 Rüschlikon, Switzerland
tel. +41 1 724 86 47
fax. +41 1 724 31 70

Prispelo (Arrived): 11.12.93 **Sprejeto (Accepted): 23.12.93**